

Short Communication

## Preparation and Properties of the Fe/N co-doped Graphene Composite Materials

Yanbo Li, Ye Wan\*, Haixiao Zhang, Xiaodan Wang

School of Materials Science and Engineering, Shenyang Jianzhu University, Shenyang 110168, China

\*E-mail: [ywan@sjzu.edu.cn](mailto:ywan@sjzu.edu.cn)

Received: 5 December 2020 / Accepted: 5 February 2021 / Published: 28 February 2021

The Fe doped and the Fe/N co-doped graphene composite materials were prepared from a graphene oxide dispersion by a hydrothermal method.  $\text{Fe}^{2+}$  was oxidized to be  $\alpha\text{-Fe}_2\text{O}_3$ , while graphene oxide was reduced to be reduced graphene oxide (rGO) during the hydrothermal reaction. For the Fe/N co-doped graphene composite material, nitrogen atoms were incorporated into the graphene structures in the form of C-N and C=N bonds. Both of the Fe doped and the Fe/N co-doped graphene composite materials exhibited a 3D hierarchical porous frame and a large surface area, which facilitated ion and electron transport. The results from electrochemical impedance spectroscopy (EIS) shows both of the charge transfer resistance and the diffusion resistance of the Fe/N co-doped material are smaller than that of the Fe doped material, which indicated that nitrogen played an important role in improving conductivity, the ion and electron transport kinetics and the redox reaction activity in the Fe/N co-doped graphene composites material.

**Keywords:** Reduced graphene oxide; Hydrothermal method; Doping; Iron oxide; EIS

### 1. INTRODUCTION

Three-dimensional macroscopic graphene hydrogel and its composites with interconnected pores have aroused continuous interests in energy storage field owing to its large surface area, rich in hierarchical pore structure, low density, good thermal stability, high electrical conductivity and good mechanical flexibility[1,2]. Once the graphene hydrogel is doped with some functionalized particles and forms a composite, it can combine the advantages of both graphene and functionalized particles. The graphene composites have widely application prospects in optoelectronic devices, energy storage, environmental protection, biology, etc[3].

However, rGO is easy to accumulate and thus affects charge transport and ion transfer process. It's known that there are numerous defects, and many groups such as C-O-OH, -C-O- and -COOH, on the surface of rGO. Metal ions might bond with those groups and support the graphene sheets. Iron

ions facilitate to bond with the groups of graphene and might improve the conductivity of graphene. Ferric oxide ( $\text{Fe}_2\text{O}_3$ ) has attracted attention in lithium ion batteries owing to its non-toxicity, high chemical stability, and high theoretical capacity[4]. A composite of  $\text{Fe}_2\text{O}_3$  and single-walled carbon nanohorns was developed via a simple hydrothermal method and the composite shows excellent electrochemical performance and cycle stability, even at a high current density of  $1000\text{mA}\cdot\text{g}^{-1}$ [4]. However, the low electrical conductivity and poor capacity retention of  $\text{Fe}_2\text{O}_3$  impede its application somehow[5].

The nitrogen-doped graphene shows different properties compared with the pristine rGO because the neighbor nitrogen atoms could influence the spin density and charge distribution of carbon atoms[6,7] and provide more active and nucleation sites[8]. Investigations have shown that nitrogen-doped graphene composite materials exhibited a high specific capacity at high current densities. Nitrogen atom doping in the graphene structure could optimize the electrode-electrolyte wettability and provide materials with good long-term stability. The hydrothermal method could provide the synthesis of nitrogen-doped graphene for various practical applications. Chen et al. synthesized macroscopic nitrogen-doped graphene hydrogels using organic amines as a nitrogen source and the prepared supercapacitor performance of the nitrogen-doped graphene hydrogels was remarkably enhanced[9]. Long et al. prepared nitrogen-doped graphene in the presence of hydrazine and ammonia when  $\text{pH} = 10$  through a colloidal dispersion of hydrothermally rGO[10].

Vanadium redox flow batteries (VRFBs), owing to their perfect combination of safety, long life cycle, stable operation and high efficiency [11-12], were used as one of the relatively ideal storage technologies and have made considerable and effective progress in the past few decades [13]. In order to obtain a more optimized graphene-based composite material, the paper utilized the one-step hydrothermal method to prepare three-dimensional macroscopic graphene composites materials doped with  $\alpha\text{-Fe}_2\text{O}_3$  (named *the Fe doped*) or co-doped with  $\alpha\text{-Fe}_2\text{O}_3$  and nitrogen atoms (named *the Fe/N co-coped*), and then investigated the electrochemical characteristic of the materials in the vanadium redox flow batteries. Graphene oxide was reduced to rGO, while  $\text{Fe}^{2+}$  was converted into  $\alpha\text{-Fe}_2\text{O}_3$  and deposited onto the graphene network during the hydrothermal process[14]. The prepared Fe/N co-doped graphene composite material not only maintains the high specific surface area of the composite, but also obtains excellent electrochemical performance.

## 2. EXPERIMENTAL

### 2.1 Preparation of the composite materials

$2\text{mg}\cdot\text{ml}^{-1}$  GO dispersion was prepared by the ultrasonic dispersal technique.  $0.24\text{ g FeC}_2\text{O}_4\cdot 2\text{H}_2\text{O}$  was added into 50 mL of the dispersion slowly. After stirred for 6 hours with a magnetic stirring apparatus, the above mixture became a uniform suspension. Then, the suspension was added with  $0.6\text{ g}$  urea and was stirred for another 2 hours again. Subsequently, the suspension was transferred to a Teflon autoclave reactor and heated for 10 hours at  $180^\circ\text{C}$ . Finally, the macro-

composite hydrogels, being obtained after the reaction mixture was cooled to room temperature, were freeze-dried and formed the Fe/N co-doped graphene composite material.

The Fe doped composite material was prepared for comparison in the same procedure as the above but without the steps that the uniform suspension was added into urea and was stirred for another 2 hours.

## 2.2 Materials characterization

The structural information of the Fe/N co-doped and the Fe-doped graphene composite materials as prepared were identified via the X-ray diffraction (XRD, Shimadzu XRD-7000, Japan) and Fourier Transform Infrared Spectrometer (FTIR, Nicolet iS5, USA). Morphological observation of the materials was carried out by using a field-emission scanning electron microscope (SEM, Hitachi S-4800, Japan). Thermogravimetry (TG) analysis was performed by using a STA-449F3 simultaneous thermal analyzer (Netzsch, Germany) in air at a heating rate of  $10^{\circ}\text{C}\cdot\text{min}^{-1}$  from  $10^{\circ}\text{C}$  to  $800^{\circ}\text{C}$ . Liquid nitrogen adsorption-desorption isotherm analysis was performed on an automatic surface area and porosimetry adsorption system (ASAP2020, USA).

## 2.3 Electrochemical tests

Cyclic voltammetry and electrochemical impedance spectroscopy (EIS) tests were carried out in a conventional three-electrode cell using a Parstat 4000+ potentiostat (Princeton Applied Research, USA) electrochemical workstation.

The solution ( $0.1\text{mol/L VO}_2\text{SO}_4+2.5\text{mol/L H}_2\text{SO}_4$ ) for the electrochemical test were supplied by Liu's research group [13].

# 3. RESULTS AND DISCUSSION

## 3.1 Structural and morphological characterization

The structural and the compositional characteristics of the materials were investigated by XRD. Fig. 1 exhibits the XRD patterns of the Fe/N co-doped and the Fe-doped graphene composite materials. The diffraction peaks at  $2\theta=24.2^{\circ}$ ,  $33.1^{\circ}$ ,  $35.6^{\circ}$ ,  $40.8^{\circ}$ ,  $49.4^{\circ}$ ,  $54.0^{\circ}$ ,  $57.5^{\circ}$ ,  $62.4^{\circ}$ ,  $64.0^{\circ}$ ,  $69.5^{\circ}$ ,  $71.9^{\circ}$ ,  $75.4^{\circ}$  and  $77.7^{\circ}$  in Fig.1(a) and (b) were ascribed to (012), (104), (110), (113), (024), (116), (122), (214), (300), (208), (1010), (220) and (306) crystal planes of  $\alpha\text{-Fe}_2\text{O}_3$  (PDF 24-0072) respectively.

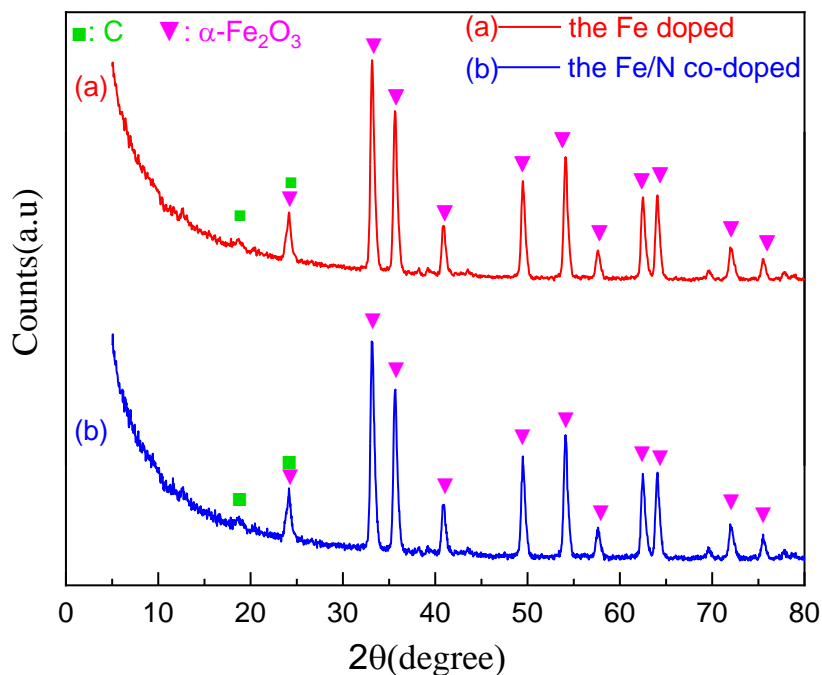


**Figure 1.** XRD patterns of the Fe/N co-doped and the Fe doped graphene composite electrolyte materials.

Those sharp peaks of  $\alpha$ -Fe<sub>2</sub>O<sub>3</sub> in Fig. 1 indicate that  $\alpha$ -Fe<sub>2</sub>O<sub>3</sub> was well crystallized in the composites and demonstrate that Fe<sup>2+</sup> provided by FeC<sub>2</sub>O<sub>4</sub>·2H<sub>2</sub>O in the suspension was oxidized to Fe<sup>3+</sup> by the graphene oxide (GO). Simultaneously, the GO was reduced to the reduced graphene oxide (rGO), which main diffraction peak is at  $2\theta=24.08^\circ$  [15] and is overlapped by the peaks of (012) plane of  $\alpha$ -Fe<sub>2</sub>O<sub>3</sub> in Fig. 1(a) and (b). Notably, no characteristic peak of graphene oxide is observed, which indicated the graphene oxides were totally reduced.

FTIR spectroscopy experiment was used to further analyze the structural properties of the Fe/N doped electrolyte materials. As depicted in Fig. 2, the characteristic bands at approximately 3600 cm<sup>-1</sup> and about 1382 cm<sup>-1</sup> are attributed to the stretching vibration of the hydroxyl group (-OH) [16]. The IR peak at around 1620 cm<sup>-1</sup> is ascribed to the stretching vibration of the carbonyl group (C=O)[17]. The band at approximately 1550cm<sup>-1</sup> is attributed to the stretching vibration of C=N group [18]. The bands at approximately 1195 cm<sup>-1</sup> and about 1105 cm<sup>-1</sup> are assigned to the stretching vibration of C-N and C-O-C respectively. The bands concerning with C-N and C=N in Fig. 2 testify that nitrogen element from urea was doped into the composite material chemically by the hydrothermal method at 180°C. Integrating the above analysis, the Fe/N co-doped graphene composite material was successful doped with both of  $\alpha$ -Fe<sub>2</sub>O<sub>3</sub> crystals and nitrogen element and named as the  $\alpha$ -Fe<sub>2</sub>O<sub>3</sub>/nitrogen co-doped graphene composite material (abbreviated as the Fe/N co-doped material), while the other as the Fe doped graphene composite material (abbreviated as the Fe doped material).

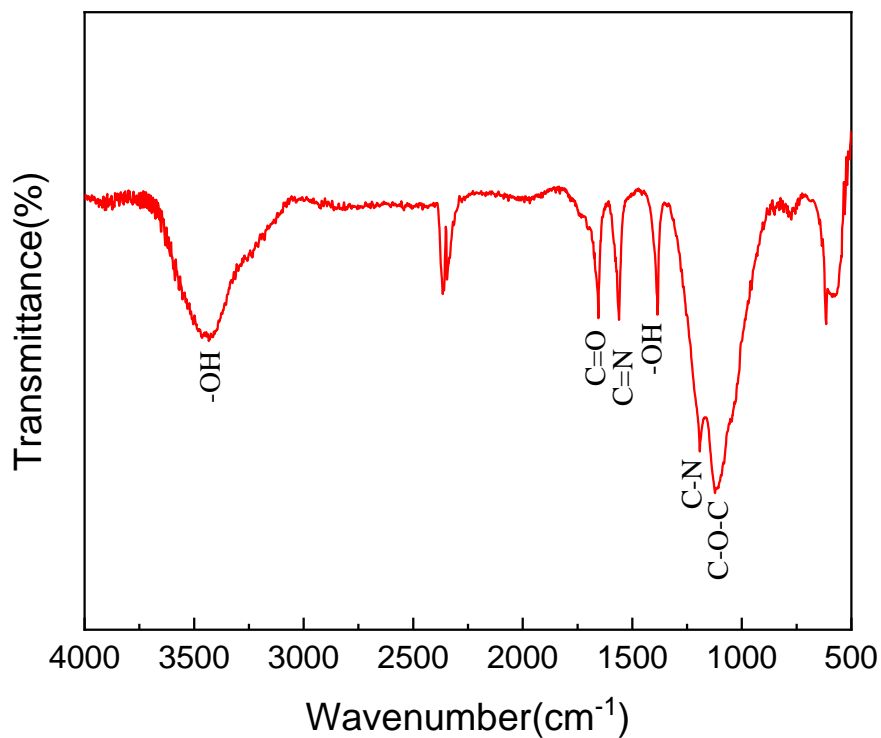


**Figure 2.** FTIR spectroscopy of the Fe/N co-doped composite material.

The surface information of the Fe-doped and the Fe/N co-doped materials was examined by using SEM (Fig. 3). It can be seen from Fig. 3 that the prepared composite materials are composed of the crumpled and aggregated multilayer nanosheets, which is consistent with the observation from Reference [17]. For both of the prepared materials, the nanosheets wrinkled and overlaid to each other and formed good three-dimensional framework structures, and then a great number of micron-sized pores were developed.

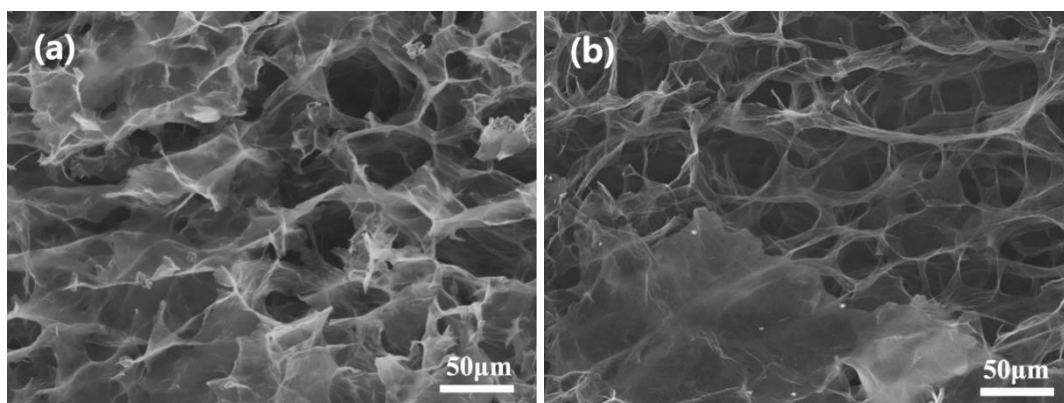


**Figure 3.** SEM images of the Fe-doped (a) and the Fe/N co-doped (b) materials.

### 3.2 Thermal characterization

Thermal stabilities of the doped composite materials were explored by thermogravimetric and differential scanning calorimeter (TG-DSC) in the air atmosphere with a heating rate of  $10^{\circ}\text{C}\cdot\text{min}^{-1}$  from  $10^{\circ}\text{C}$  to  $800^{\circ}\text{C}$ , as shown in Fig. 4.

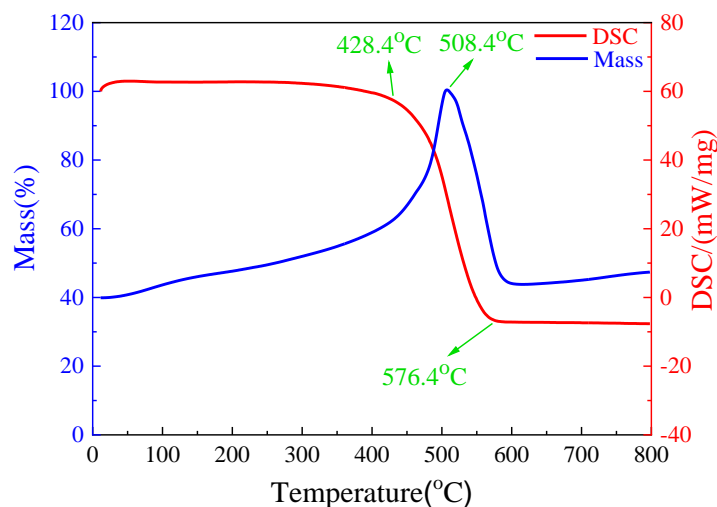


**Figure 4.** Simultaneous TG-DSC curves of the Fe/N co-doped material in air. The temperature was controlled from  $10^{\circ}\text{C}$  to  $800^{\circ}\text{C}$  and the heating rate is programmed at  $10^{\circ}\text{C}\cdot\text{min}^{-1}$ .

A great weight loss at the temperature between  $428.4^{\circ}\text{C}$ ~ $576.4^{\circ}\text{C}$  can be observed. Notably, the sharp weight loss is accompanied by a strong exothermic peak at  $508.4^{\circ}\text{C}$ , which illustrates the decomposition of a component of the Fe/N co-doped material. According to the results of Fig. 1 and Fig. 2, the Fe/N co-doped material is composed of graphene,  $\alpha\text{-Fe}_2\text{O}_3$  and organic components containing the C-N and the C=N bonds. Therefore, the strong exothermic peak at  $508.4^{\circ}\text{C}$  should be attributed to the decomposition of graphene, and the mass loss is corresponding ascribed to removal of small molecules resulting from the decomposition of graphene. The slight weight loss at the temperature from  $60^{\circ}\text{C}$  to  $110^{\circ}\text{C}$  is assigned to the removal of the small molecules, such as adsorbed water and carbon dioxide.

The mass and the exothermic curves are near constant and when the temperature is over  $576.4^{\circ}\text{C}$ , which indicated the remnant is  $\alpha\text{-Fe}_2\text{O}_3$ . It can be observed from Fig. 4 that the mass percentage of  $\alpha\text{-Fe}_2\text{O}_3$  in the Fe/N co-doped material was approximately 32.7wt %.

### 3.3 Electrochemical characterization

To gain an insight into the electrochemical characterization, the electrochemical behaviors of the prepared materials were studied in  $0.1\text{mol/L VOSO}_4+2.5\text{mol/L H}_2\text{SO}_4$  by using the cyclic voltammetry (CV) technology in a conventional three electrode cell. Fig. 5 shows the CV curves of the Fe doped and the Fe/N co-doped materials obtained at a scan rate of  $10\text{mV}\cdot\text{S}^{-1}$  through the voltage range from  $0\sim 0.8\text{ V}_{\text{SCE}}$ . It is obvious that the CV curves of the two doped materials are symmetric pseudo-rectangle, which indicates both of the materials exhibiting high capacity characteristics [19].

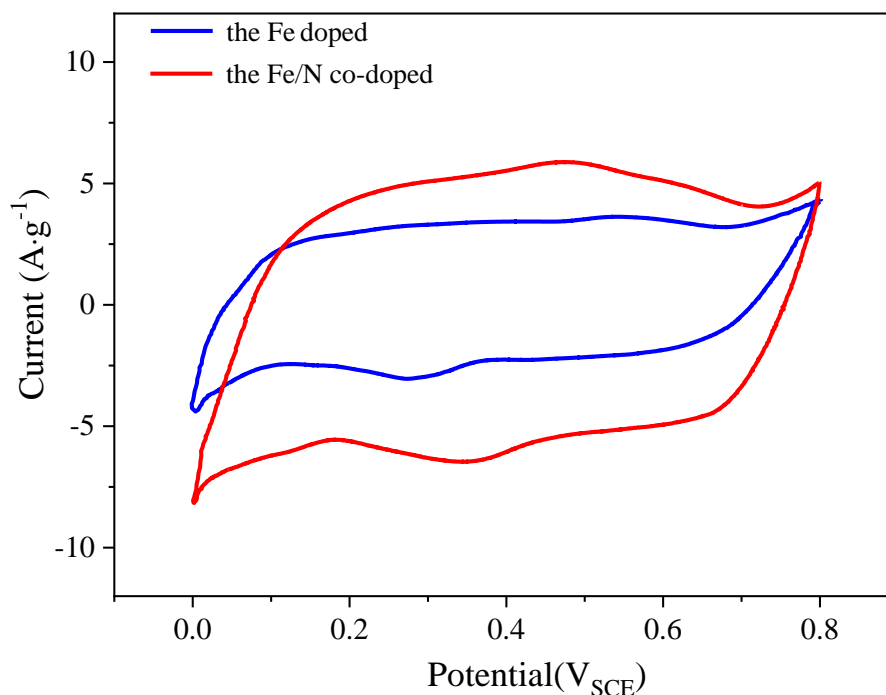


**Figure 5.** Cyclic voltammetry curves of the Fe doped and the Fe/N co-doped materials in 0.1mol/L  $VOSO_4$ + 2.5mol/L  $H_2SO_4$  solution at a scan rate of 10  $mV s^{-1}$ .

It can be seen from Fig. 5 that there are a pair of redox peaks in each curve. The peak current of the Fe/N co-doped electrode is greater than the Fe doped electrode, which implies that the redox reactions of the  $VO_2^+/VO^{2+}$  at the electrode surface were enhanced by the nitrogen atoms doped into the graphene composite material, and thus enhance the reaction activity and the reaction current. It can be observed that the redox potential difference of the Fe/N co-doped electrode reduced approximately 0.12 V than that of the Fe doped electrode, which suggests the doped nitrogen atoms raised the redox reversibility of the electrode.

EIS analysis was further carried out to reveal the electrochemical reaction kinetics of the electrolytical ions into/out of the Fe doped and the Fe/N co-doped electrodes. The Nyquist plots of the two electrodes are shown in Fig. 6 and the charge transfer resistance during the redox reactions and the resistance of diffusion during the reaction processes.

It is obvious from Fig. 6 that each curve was comprised of a semicircle in the high-frequency region and a straight line in the low-frequency, which are corresponding to the charge transfer process and the mass transfer process respectively[17,19-20]. The charge transfer resistance, illustrated by the radius of the semicircle, of the Fe/N co-doped electrode is approximately  $45.9\Omega$ , which is much smaller than that of the Fe doped electrode (around  $133.2\Omega$ ). The smaller charge transfer resistance toward positive and negative redox reactions, meaning a better  $VO_2^+/VO^{2+}$  and  $V^{2+}/V^{3+}$  redox kinetics, is favorable for the charge transfer and the electrochemical reaction for the Fe/N co-doped electrode.

The slope of the straight line in the low-frequency region is associated with the Warburg impedance and related to the diffusion of electrolytical ions in electrodes. The slope of the Fe/N doped

electrode is greater than that of the Fe doped electrode, which indicates a better conductance with a smaller ion transfer resistance in the Fe/N doped electrode than in the Fe doped electrode. From the high-frequency and the low-frequency information of the EIS curves in Fig. 6, it can be drawn that the Fe/N co-doped electrode performed higher electrochemical activity and conductivity than the Fe doped electrode owing to the doped nitrogen atoms increased the charge mobility[8, 21] and rendered a favorable conductivity of the electrode.

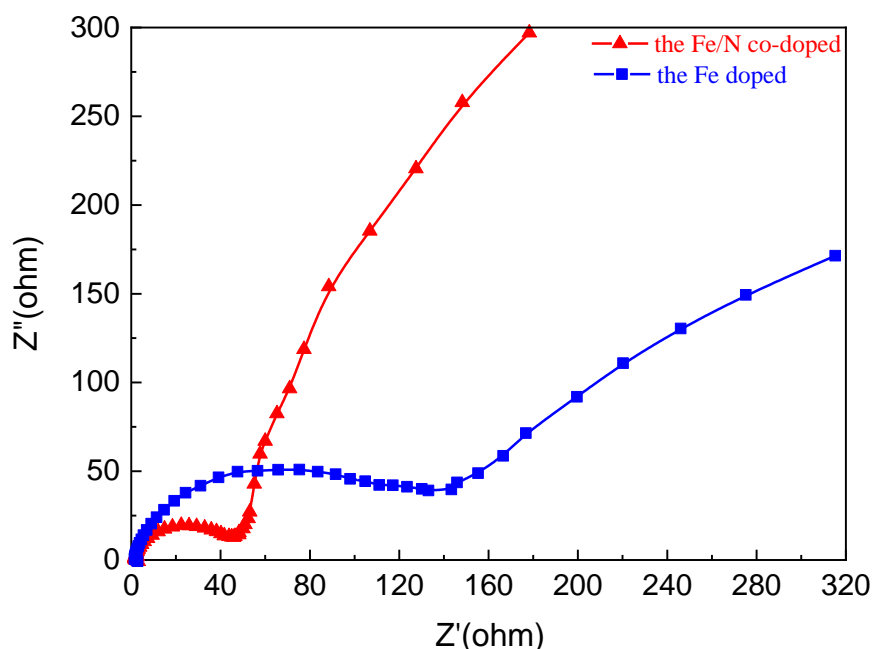


**Figure 6.** EIS diagrams of the Fe/N co-doped and the Fe doped electrodes in 0.1mol/L  $\text{VO}_2\text{SO}_4$ +2.5mol/L  $\text{H}_2\text{SO}_4$  electrolyte at a test frequency range of 0.1~100kHz.

The graphene hydrogel exhibits fine adsorbability. The adsorbed  $\text{Fe}^{2+}$  ions were further oxidized to be  $\text{Fe}^{3+}$ , which bonded with oxygen atom to be  $\alpha\text{-Fe}_2\text{O}_3$  crystals during the following hydrolysis and freeze-dried procedures.  $\alpha\text{-Fe}_2\text{O}_3$  disperses uniformly in the graphene hydrogel and help support the 3D frame of the rGO nanosheets.

It can be seen from Fig. 3, there are numerous pores in the rGO, which not only were diffusion channels and beneficial for the access of an electrolyte but also provided a larger reaction contact area for the electrolyte ions. Furthermore, the doped  $\alpha\text{-Fe}_2\text{O}_3$  crystals provided more reactive sites for the rGO, and hence improved the catalytic activity and the efficiency of the electrode.

For the Fe/N co-doped material, owing to the doped nitrogen atoms, there were many crystal defects in the graphene and increased the numbers of the unsaturated carbon atoms, and thus favored for their bonding with oxygen [22]. On the other hand, the nitrogen atoms doped into the carbon cyclic can change the spin density of the charges of the adjacent carbon atoms[6,7], which can adsorb oxygen atoms and the reaction intermediates and hence enhance the redox catalytic activity of the electrode, which can be seen in Fig. 5 and 6.

#### 4. CONCLUSIONS

The Fe doped and the Fe/N co-doped graphene composite materials were synthesized by using the spontaneous redox reaction between  $\text{Fe}^{2+}$  and graphene oxide by one-step hydrothermal procedure. Iron atoms are doped as  $\alpha\text{-Fe}_2\text{O}_3$  in the graphene composite materials and nitrogen in the form of C=N and C-N bonds.

Both of the charge transfer resistance and the diffusion resistance of the Fe/N co-doped graphene composite material are smaller than that of the Fe doped graphene composite material, which indicated that the nitrogen atoms play an important role in improving the ion and electron transport kinetics and improving the redox reaction.

#### ACKNOWLEDGEMENTS

This work was financially supported by the Liaoning Revitalization Talent Program (XLYC200xxxx), Scientific Research Fund of Liaoning Provincial Education Department (LNZD201905) and Scientific Research Fund of Liaoning Provincial Education Department (LNJC202016)

#### DECLARATION OF INTEREST

The authors do not have conflicts of interest in the publication of this manuscript.

#### References

1. J. Zhu, L. R. Kong, X. P. Shen, Q. R. Chen, Z. Y. Jia, J. H. Wang, K. Q. Xu, G. X. Zhu, *Appl. Surf. Sci.*, 428 (2018) 348.
2. R. Mukherjee, A. V. Thomas, A. Krishnamurthy, N. Koratkar, *ACS Nano*, 6 (2012) 7867.
3. R. Raccichini, A. Varzi, S. Passerini, B. Scrosati, *Nat. Mater.*, 14 (2015) 271.
4. Y. Zhao, J. Li, Y. Ding, L. Guan, *Chem. Commun.*, 47 (2011) 7416.
5. X. J. Zhu, Y. W. Zhu, S. Murali, M. D. Stollers, R. S. Ruoff, *ACS Nano*, 5 (2011) 3333.
6. H. B. Wang, T. Maiyalagan, X. Wang, *ACS Catal.*, 2 (2012) 781.
7. Y. H. Cao, H. Yu, J. Tan, F. Peng, H. J. Wang, J. Li, W. X. Zheng, N. B. Wong, *Carbon*, 57 (2013) 433.
8. M. Du, C. H. Xu, J. Sun, L. Gao, *Electrochim. Acta*, 80 (2012) 302.
9. P. Chen, J. J. Yang, S. S. Li, Z. Wang, T. Y. Xiao, Y. H. Qian, S. H. Yu, *Nano Energy*, 2 (2013) 249.
10. D. H. Long, W. Li, L. C. Ling, J. Miyawaki, I. Mochida, S. H. Yoon, *Langmuir*, 26 (2010) 16096.
11. J. Ye, Y. Cheng, L. Sun, M. Ding, C. Wu, D. Yuan, X. Zhao, C. Xiang, C. Jia, *J. Membr. Sci.*, 572 (2019) 110.
12. L. Zeng, J. Y. Ye, J. H. Zhang, J. Liu, C. K. Jia, *Surf. Coat. Technol.*, 358 (2019) 167.
13. Z. Y. Xu, W. Xiao, K. Y. Zhang, D. H. Zhang, H. Wei, X. H. Zhang, Z. Y. Zhang, N. W. Pu, J. G. Liu, C. W. Yan, *J. Power Sources*, 450 (2020) 227686
14. J. F. Wu, A. A. Zhou, Z. F. Huang, L. Li, H. Bai, *Chinese J. Chem.*, 34 (2016) 67.
15. H. J. Shin, K. K. Kim, A. Benayad, S. M. Yoon, H. K. Park, I. S. Jung, M. H. Jin, H. K. Jeong, J. M. Kim, J. Y. Choi, Y. H. Lee, *Adv. Funct. Mater.*, 19 (2009) 1987.
16. L. Zhang, Y. Li, Han Guo, H. H. Zhang, N. Zhang, T. Hayat, Y. B. Sun, *Environ. Pollut.*, 248 (2019) 332.
17. Y. B. Sun, S. B. Yang, Y. Chen, C. C. Ding, W. C. Cheng, X. K. Wang, *Environ. Sci. Technol.*, 49 (2015) 4255.

18. P. Su, H. L. Guo, S. Peng, S. K. Ning, *Acta Phys.-Chim. Sin.*, 28 (2012) 2745
19. W. S. Du, Y. K. LÜ, Z. W. Cai, C. ZHANG, *Acta Phys-Chim. Sin.*, 33 (2017) 1828.
20. M. V. Reddy, T. Yu, C. H. Sow, Z. X. Shen, C. T. Lim, G. V. S. Rao, B. V. R. Chowdari, *Adv. Funct. Mater.*, 17 (2007) 2792.
21. H. L. Wang, Y. Y. Liang, T. Mirfakhrai, Z. Chen, H. S. Casalongue, H. J. Dai, *Nano Res.*, 4 (2011) 729.
22. R. E. Williford, J. G. Zhang, *J. Power Sources*, 194 (2009) 1164.

© 2021 The Authors. Published by ESG ([www.electrochemsci.org](http://www.electrochemsci.org)). This article is an open access article distributed under the terms and conditions of the Creative Commons Attribution license (<http://creativecommons.org/licenses/by/4.0/>).